Symmetry breaking perturbative flows to retrieve resonant modes in plane shear layers

Takeshi Akinaga[a,c], Tomoaki Itano[b], Sotos Generalis [c,*]

[a] *Marie Sklodowska Curie International Incoming Fellow*
[b] *Department of Pure and Applied Physics, Faculty of Engineering Science, Kansai University, Osaka 564-8680, Japan*
[c] *System Analytics Research Institute, Aston University, Birmingham, B4 7ET, United Kingdom*

Abstract

We propose a simple computational procedure in order to resolve the degeneracy, which invariably exists on the background of fluid motion associated with a channel of infinite extent. The procedure is applied to elucidate the bifurcation structure for the particular case of laterally heated flow with the addition of a perturbative Poiseuille flow component. The introduction of a symmetry breaking perturbation as the simplest imperfection alters the bifurcation tree of the original shear flow. As a result, the previously unknown higher order nonlinear solutions for the unperturbed flow are discovered, without implementing classical stability theory.

Keywords: Bifurcation, nonlinear stability, 2:1 resonance, homotopy, symmetry breaking perturbation
PACS: 47.10. -g

1. Introduction and Methodology

It is well known in quantum mechanics that a spectral line composed by different components can be split under the presence of a static perturbative magnetic field. This fact, the so-called Zeeman effect, implies that multiple

*Corresponding author
Email addresses: s.c.generalis@aston.ac.uk (Sotos Generalis), s.c.generalis@aston.ac.uk (Sotos Generalis)

orbits of an electron can be generated with the introduction of a perturbation. Similarly in this study, we show that degenerate states of shear flow can be detected with the introduction of a computational perturbation.

Turbulent channel flow is not only one of the fundamental themes pursued in the field of fluid physics, but also of great engineering importance. Historically, attempts to computationally model turbulent flow and understand its origins, structure and evolution were based on statistical approaches. Since the details of the aperiodicity (in velocity fields for example) observed in experiments or in numerical simulations are not of prime interest, one usually tries to characterise turbulent systems by their statistical and time averaged properties. Although it is widely accepted that the Navier-Stokes equations should provide the correct basis for an accurate description of turbulent fluid flow, it is regrettable that rather little information from the equations, enters into the statistical analysis.

More recently, the sequence of bifurcations/deterministic approach has emerged as a popular tool due to the discovery of coherent solutions that are universal. They exist in a variety of fluid flows as invariant sets within the turbulent regime and they have been obtained without the presumption of favourable or pre-set conditions deduced from empirical laws. Moreover the discovery of coherent structures indicates the existence of order within the evident aperiodicity of turbulence, that in turn could be used to probe aperiodic motion in a deterministic way. Therefore the sequential bifurcation approach, that identifies coherent structures and examines their stability, can potentially overcome many difficulties associated with transitions to turbulence.

In order to describe in general terms the sequential bifurcation approach that will be followed in the next sections, we introduce the governing equation of fluid motion:

$$\frac{\partial \boldsymbol{u}}{\partial t} + \boldsymbol{L}(\boldsymbol{R})\,\boldsymbol{u} + \boldsymbol{N}(\boldsymbol{u}) = \boldsymbol{0}. \tag{1.1}$$

In the set of partial differential equations (1.1) $\boldsymbol{u}$ describes the deviation from the basic (undisturbed) state of the system, $\boldsymbol{L}(\boldsymbol{R})$ is a linear and $\boldsymbol{N}(\cdot)$ is a nonlinear operator that involve partial derivatives. In (1.1) $\boldsymbol{R}$ represents collectively the parameters of the system, such as the Prandtl, the Rayleigh or the Reynolds numbers. In our sequential bifurcation approach we will be employing (1.1) and we first obtain the stability of the basic state via the introduction of infinitesimal disturbances in (1.1) and by ignoring the nonlinear terms. The nonlinear states grow from the stability boundary of

the basic state, that is typically characterised by $f(\boldsymbol{R}) = 0$, where f is the neutral surface of the basic state. If we repeat the aforementioned procedure of perturbation on the obtained nonlinear states, we could find a successive sequence of bifurcations for the higher order states en route to turbulence.

We intend to deduce, or identify, numerically coherent structures for given values of the control parameters, for the case when the fluid is interacting with plates of infinite extent. This is because the flow, in this case, is free from the influence of the presence of end boundaries at inlet or the outlet in the upstream and donwstream ends of the channel. Additionally the proposition of the infinite channel allows the introduction of Fourier expansions into the simulations for the streamwise and spanwise directions.

From the theoretical viewpoint, let us suppose a numerical channel with the gap width, $2h$, under the periodic boundary conditions with wave numbers α and β in the streamwise and spanwise directions.This channel is the subspace of another numerical channel with the same gap width but with (subharmonic) wave numbers $\frac{1}{m}\alpha$ and $\frac{1}{n}\beta$, where n, m are arbitrary positive integers. An exact equilibrium state realised in the fundamental channel is definitely an exact state in the subharmonic channel.The latter exact state may bifurcate from the former exact state, which is traditionally termed as the subharmonic bifurcation. Taking an infinite number of the combinations (m, n) into account, multiplicity of the exact states exists inevitably in the channel with infinite extent. In this manuscript we will provide an example of how to probe previously unexplored subharmonic branches by a simple perturbation, without the traditional approach of linear stability analysis using Floquet parameters.

In the following section, we formulate the problem and identify the basic state determined uniquely from the homogeneous external conditions. We obtain the stability boundary of the basic state in section 3, and proceed to solve (1.1), thus establishing the fully nonlinear solutions up to and including the tertiary level in the sequence of bifurcations approach to turbulence. We conclude this manuscript with a general discussion of our results and future work.

2. Formulation

We consider an incompressible Boussinesq Newtonian fluid bounded between two vertical parallel plates of infinite extent with different temperatures

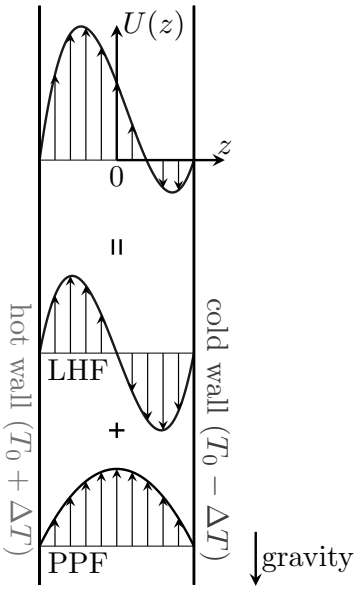

Figure 2.1: Geometrical configuration of the problem. The antisymmetric profile for pure Laterally Heated Flow (LHF) deviates from the exactly antisymmetric form under a small perturbation induced by the mean pressure deviation induced in the streamwise direction by the Poiseuille flow component.

$T_0+\Delta T$ and $T_0-\Delta T$, subject to a pressure gradient deviation from the hydrostatic pressure, see Fig. 2.1. The origin of the Cartesian coordinates system is positioned in the midplane of the fluid layer of width $2d$, taking x, y, z as the streamwise, spanwise and wall normal directions with unit vectors $\hat{\boldsymbol{i}}$, $\hat{\boldsymbol{j}}$, $\hat{\boldsymbol{k}}$. We assume here the state satisfies the periodic boundary conditions with wave numbers α and β for the x and y directions, respectively. The velocity $\boldsymbol{v}$ and the temperature T are governed by the following equations:

$$\frac{\partial}{\partial t}\boldsymbol{v} + \boldsymbol{v}\cdot\boldsymbol{\nabla}\boldsymbol{v} = -\frac{1}{\rho}\boldsymbol{\nabla}\pi + g\,\gamma\,T\,\hat{\boldsymbol{i}} + \nu\boldsymbol{\nabla}^2\boldsymbol{v}, \tag{2.2}$$

$$\frac{\partial}{\partial t}T + \boldsymbol{v}\cdot\boldsymbol{\nabla}T = \kappa\,\boldsymbol{\nabla}^2 T, \tag{2.3}$$

$$\boldsymbol{\nabla}\cdot\boldsymbol{v} = 0, \tag{2.4}$$

where we have incorporated the hydrostatic pressure term $g\gamma T_0 x$ in π. Here ρ is the density, κ is the thermal diffusivity, ν is the kinetic viscosity, γ is the coefficient of thermal expansion and g is the acceleration due to gravity. For the non-dimensional description of the problem we use d, d^2/ν and $\Delta T/PrGr$, as the units of length, time and temperature, respectively. The physical properties of the system are characterised by the three non-dimensional parameters $Gr = g\gamma\Delta T d^3/\nu^2$, the Grashof number that gives the strength of the heating, $R = U_{max}d/\nu$, the Reynolds number that measures the strength of the applied pressure gradient in the streamwise direction (U_{max} is the speed of Poiseuille laminar flow at the origin) and the Prandtl number $Pr = \nu/\kappa$. Taking the non-dimensional form of the velocity, temperature and pressure deviations from the basic state as $\boldsymbol{u}$, θ and Π, we obtain the non-dimensional form corresponding to (2.2)-(2.4),

$$\frac{\partial}{\partial t}\boldsymbol{u} + \boldsymbol{u}\cdot\boldsymbol{\nabla}\boldsymbol{u} = -\boldsymbol{\nabla}\,\Pi + \theta\,\hat{\boldsymbol{i}} + \boldsymbol{\nabla}^2\boldsymbol{u}, \tag{2.5}$$

$$\frac{\partial}{\partial t}\theta + \boldsymbol{u}\cdot\nabla\theta = Pr^{-1}\boldsymbol{\nabla}^2\theta, \tag{2.6}$$

$$\boldsymbol{\nabla}\cdot\boldsymbol{u} = 0. \tag{2.7}$$

Hereafter, we restrict the scope of our study to the case of $Pr = 0$ and two-dimensional flow (no spanwise dependence of the flow), so that our primary motivation in the present study, the retrieval of resonant modes, via the introduction of symmetry breaking perturbative flows, may be realised simply. At the vanishing limit of Pr, the conductivity of temperature is predominant against inertia, the energy equation (2.6) decouples from the momentum equation (2.5) and the temperature variation becomes simply proportional to z independently from $\boldsymbol{u}$. The basic solution of equations (2.5)-(2.7), which satisfies the no-slip condition for the velocity ($\boldsymbol{u} = 0$) on the boundaries at $z = \pm 1$, is given by:

$$\boldsymbol{U}_{\mathrm{B}}(z) = U_0(z)\,\hat{\boldsymbol{i}},\ U_0(z) = (Gr/6)(z^3 - z) + R(1 - z^2). \tag{2.8}$$

For the configuration of Figure 2.1 Squire's theorem is applicable (see Squire (1933)). We further assume that the pressure gradient remains in the mean unchanged by the amplitude of the secondary flow and we show that there exists degeneracy that is invariably linked with the possibility of infinite streamwise length. In order to obtain the fully nonlinear equilibrium solution of these two-dimensional rolls we introduce the stream function ψ, a function

of (x, z)-variables, with the velocity fluctuations $\widetilde{\boldsymbol{u}}$ satisfying:

$$\widetilde{\boldsymbol{u}} = \nabla \times \psi \, \hat{\boldsymbol{j}}. \tag{2.9}$$

The boundary conditions for ψ are given by:

$$\psi = \frac{\partial \psi}{\partial z} = 0 \quad \text{at} \quad z = \pm 1. \tag{2.10}$$

Two-dimensional steady equilibrium roll solutions were therefore sought numerically employing the Chebyshev Gauss-Lobatto collocation point method combined with the Newton-Raphson iterative method via the following harmonic expansion for ψ:

$$\psi(x, z, t) = \sum_{n=0}^{N} \sum_{m=-M,\ m\neq 0}^{M} a_{nm} \ \left(1 - z^2\right)^2 \ T_n(z) \ \mathrm{e}^{\mathrm{i}m\,\alpha(x-ct)}, \tag{2.11}$$

where N and M are the truncation levels for the complex coefficients a_{nm}, and $T_n(z)$ is the n-th order Chebyschev polynomial. We have incorporated the phase velocity c in the expansion, so that we can examine additionally the case, where a perturbative Poiseuille flow component is allowed to be present in the configuration of Figure 2.1, via the implementation of $R \neq 0$ in (2.8). In this case calculations are performed on a moving frame that is phase locked with the nonlinear solutions bifurcating from the neutral curve boundaries. The factor $(1 - z^2)^2$ has been inserted in the expression for ψ in order to take into account the boundary conditions expressed by eqs. (2.10).

By substituting the expansion (2.11) into the streamwise projection of the curl of (2.5), multiplying the resulting equations by $\int_0^{2\pi/\alpha} dx \, \mathrm{e}^{\mathrm{i}l\,\alpha\,x}$, $l = 1, 2, \ldots$, we can evaluate the expansions (2.11) at each collocation point, i.e. we obtain a set of nonlinear algebraic equations for the complex coefficients a_{nm}. Further details of the numerical method employed here to obtain nonlinear solutions have been presented recently in Generalis and Fujimura (2009) and Itano and Generalis (2009); Generalis and Itano (2010) in relation to different types of shear flows. We elaborate on the results of our simulations in the next section.

3. Results

3.1. Linear stability

We define the neutral stability curve, as the curve that provides the critical Gr number as a function of the wavenumber α at a pre-specified

value of Reynolds number say, $Gr_{\rm c}(\alpha, R)$. In Figure 3.2, the neutral curve $Gr = Gr_{\rm c}(\alpha, R = 0)$, is given as a thick solid curve on the α-Gr plane. The thin solid curves on the left hand side of the α-Gr plane are also neutral curves, but they depict the $Gr_{\rm c}(n\alpha, 0)$ relationship in the case, where the scale of α has been reduced by a factor $1/n$, n $= 2, 3, 4$. These are described by the functional relationship $Gr = Gr_c(n\alpha)$ and we term them subharmonic neutral stability curves. At a given $Gr > Gr_{\rm c}(n\alpha, 0)$, an infinitesimal disturbance added onto the basic flow may grow exponentially. The eigen function generated from $Gr_{\rm c}(\alpha, 0)$ is referred to as the fundamental mode, while those from the duplications $Gr_{\rm c}(n\alpha, 0)$ $(n = 2, 3, 4)$ are referred to as subharmonic modes.

Table 3.1: Wavenumber and Grashof number at bi-critical point, $(\alpha_{{\rm c},n}, Gr_{{\rm c},n})$, at $R = 0$ are listed, which are determined as the solution of $Gr_{\rm c}(\alpha, 0) = Gr_{\rm c}(n\alpha, 0)$. At the bi-critical point, the nonlinear branch may be generated from a certain noninear interaction between the fundamental and subharmonic modes. For example, the branch T shown in Fig. 3.2 originates at a second bi-critical point, $(\alpha_{\rm c,2}, Gr_{\rm c,2})$, listed in Tab.3.1.

n	$\alpha_{{\rm c},n}$	$Gr_{{\rm c},n}$
2	0.8631	604.3
3	0.6166	791.9
4	0.4761	999.9
5	0.3879	1212.7
6	0.3277	1426.1
7	0.2839	1639.1
8	0.2506	1851.9

3.2. Resonance in the infinite extent case

Since we assumed that the system has an infinite extent, it is necessary to keep in mind the fact that the characteristic wavelength is selected by nature, that is, the wavelength dominating the bifurcating nonlinear state should not be pre-assumed by our calculations. It is possible that any combination that consists of a number of eigenmodes, associated with the neutral curves, can develop into some resonant nonlinear state in the system with infinite extent.

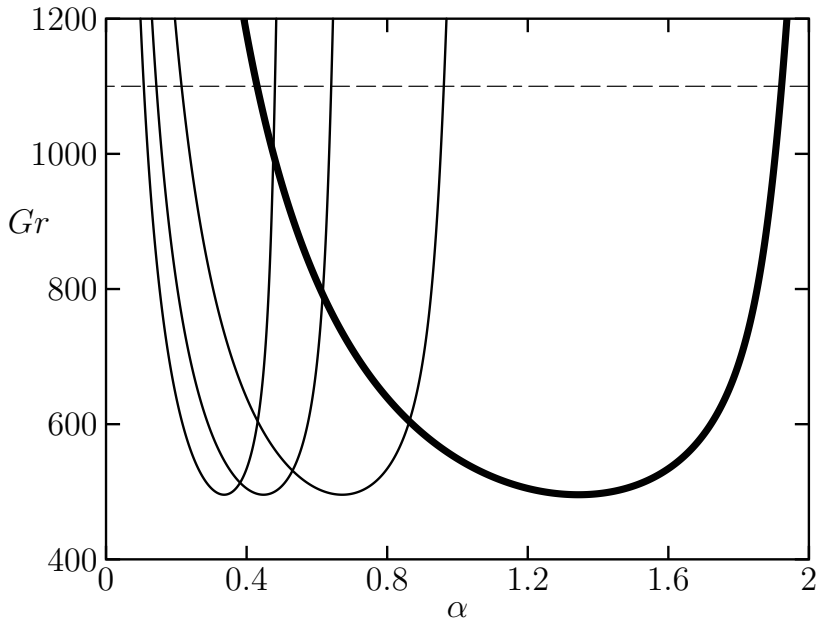

Figure 3.2: The neutral curves for the fundamental (solid) and subharmonic modes (dashed) at $R = 0$, which is described as $Gr = Gr_c(n\alpha, 0)$ $n = 1, 2, 3, 4$. The critical Grashof number is $Gr = 495.6$ at the wavenumber $\alpha = 1.344$. The intersections of the curves, which are termed as "bi-critical points", are all candidates of the origins for the nonlinear states generated by a certain nonlinear interaction between the different modes, the pure (nonlinear states from the neutral curve) and the subharmonic neutral curves. This is the so called "resonance".

The case of the conventional Rayleigh Benard convection is an example, where, square or hexagonal cells are constituted by the combination of two or three self resonating eigenmodes. In Table 3.1, we list the specific parameter values (α, Gr), for the "bi-critical points", at which the neutral stability curve intersects the subharmonic stability curves, $Gr_c(\alpha) = Gr_c(n\alpha)$ $(n > 1)$. At these parameter values the fundamental mode may interact the subharmonic modes, so that a non-linear state can be established.

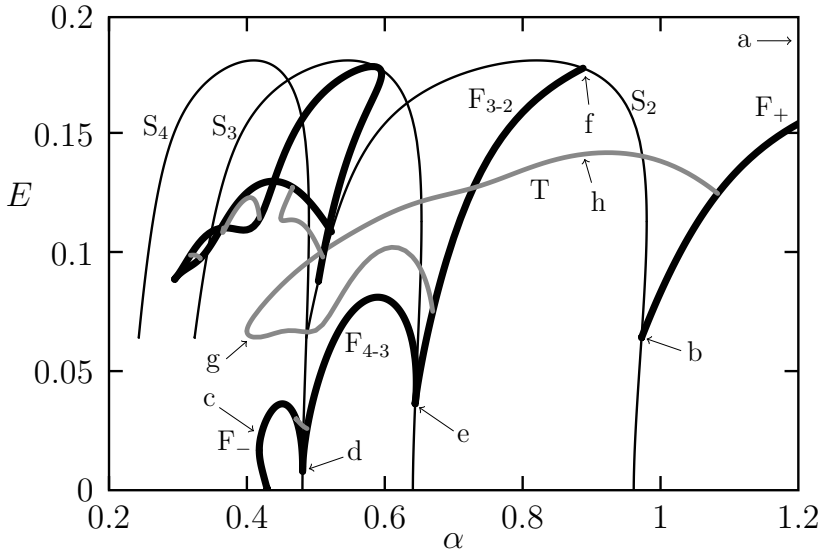

Figure 3.3: Nonlinear branches at $(Gr, R) = (1100, 0)$. The thick curves marked by $F_{\pm}$ is the secondary branches bifurcated directly from the basic state on the neutral curve, $Gr = Gr_{\rm c}(\alpha, 0)$. In particular, the curve marked F_- connects to those of F_{4-3} and F_{3-2} sequentially on the thin curves with S_n, which refer to the n-th subharmonic duplications of the F_+. The gray curve with symbol T and the other gray curves depicted in the left hand side of the graph correspond to the travelling wave solutions obtained in the present procedure. The lower case corresponds the location in the graph where the corresponding flow pattern illustrated in the Fig.3.4 are obtained.

3.3. Previous work

Previous studies on the subject have remained an ambiguous point in their attempts to clarify the nature of the interaction that the fundamental and subharmonic modes play, as well as the crucial role that these interactions play for a system with infinite extent as a whole. For the case of $R = 0$, as in the present model, Nagata and Busse (1983) calculated equilibrium states, which should be expected to bifurcate from $Gr_{\rm c}(\alpha, 0)$, but the finite-amplitude equilibrium states were obtained only for a narrower range than expected. Let us explain this. Suppose that the laminar state looses its stability at a given Gr against a perturbation with the wave number α satisfying $\alpha_- < \alpha < \alpha_+$, where $\alpha_{\pm}$ are the solutions of $Gr = Gr_{\rm c}(\alpha, 0)$.

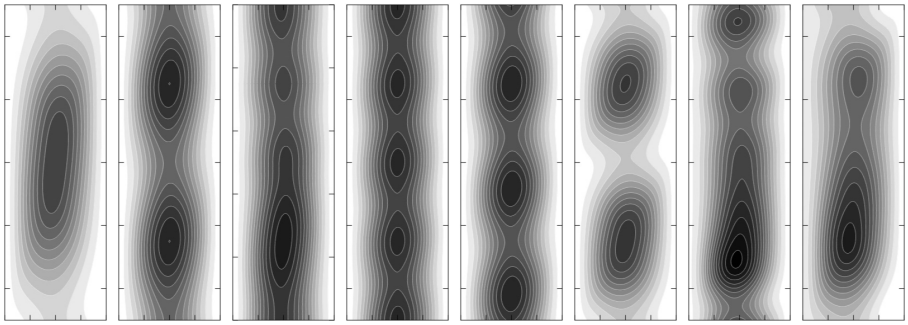

Figure 3.4: Contour plots for stream function for $Gr = 1100,\ \ R = 0$. The contour levels are indicated in light grey scale for small and in dark grey scale for large values and for: (a) $\alpha = 1.60$ on F_+, (b) $\alpha = 0.98$ on F_+, (c) $\alpha = 0.42$ on F_-, (d) $\alpha = 0.48$ on F_-, (e) $\alpha = 0.64$ on F_{4-3}, (f) $\alpha = 0.88$ on F_{3-2}, (g) $\alpha = 0.42$ on T, (h) $\alpha = 0.88$ on T. In each plot the state between the boundaries is depicted for one wavelength in the ordinate. The location (a)-(h) of the corresponding flow pattern in the (α, Gr) plane is indicated in Fig.3.3.

Fujimura and Mizushima (1987) claimed that the equilibrium state can exist only in the range of wave number $\alpha_+/2 < \alpha < \alpha_+$. Fujimura and Mizushima (1987) could partly explain the mystery mentioned above. Employing weakly nonlinear analysis, they showed the possibility that an interaction of the fundamental mode with the subharmonic mode may constitute a nonlinear equilibrium state with subharmonic wave number, which could not be obtained in Nagata and Busse (1983). The case of Rayleigh-Benard convection was also reported in Busse and Clever (1974) and Mizushima and Fujimura (1992). In Mizushima and Fujimura (1992) the discrepancy in the bifurcation diagram of Nagata and Busse (1983) was accounted for, by attributing one of the 'hidden' states as the state generated by the mutual interaction between the fundamental and subharmonic modes n $(= 2, 3, 4, \cdots)$. This was termed as $1 : n$ resonance, according to them.

3.4. Unravelling the mystery of the resonant region

By introducing to the system with infinite extent a perturbation breaking the symmetry of the basic state, we will obtain possible resonant nonlinear

states at $Gr = 1100$ and $R = 0$ (see Fig. 3.3 (a)). Following Herbert (1980), we characterise states in terms of the kinetic energy of the fluctuation normalised with respect to the basic flow, E,

$$E = \sum_{m=1}^{m=\infty} E_m, \quad E_m = \frac{15}{8} \int_{-1}^{+1} \int_{0}^{2\pi/\alpha} |\nabla \psi_m|^2 \, dx \, dz, \quad \psi_m = \sum_{n=0}^{N} \psi_{nm} + \text{c. c.} \tag{3.12}$$

In Fig. 3.3, the secondary branches bifurcated from the neutral curve $Gr_c(\alpha, 0)$ at $\alpha = \alpha_\pm$ for $Gr = 1100$ are depicted as thick curves with symbol $\mathrm{F}_\pm$. $\mathrm{F}_\pm$ stands for the secondary state that bifurcates from the *fundamental* neutral curve at $\alpha_\pm$. The three thin curves, S_n, are duplications with scale factors n $(= 2, 3, 4)$ from F_+. S_n stands for the secondary state that bifurcates from the *subharmonic* neutral curve at $\alpha_\pm/n$. T stands for a tertiary (travelling wave) state bifurcated from the secondary states.

Branch F_+ bifurcated from $\alpha_+ (= 1.922)$ terminates at the node on S_2, $\alpha = 0.973$. Along the F_+ as α decreases, the flow pattern changes from single vortex state (Fig. 3.4(a)) to two vortex state (Fig. 3.4(b)). On the other hand F_- bifurcated from $\alpha_- \ (= 0.430)$ terminates at $\alpha = 0.481$ on S_4. Along the F_- as α increases, the flow pattern changes from single vortex state (Fig. 3.4(c)) to four vortex state (Fig. 3.4(d)). The branch F_- joins with a branch F_{34} at $\alpha = 0.481$ on S_4, and F_{34} connects to a branch F_{23} at $\alpha = 0.644$ on S_3. F_{mn}, m, n integers, refers to the nonlinear state bifurcated from the neutral curve that exists in the m, n resonant region. At the node on S_n n vortex state (Fig. 3.4(d)-(f)) is observed. Finally, F_{3-2} terminates at the node at S_2. There is only the branch S_2 between $\alpha = 0.888$ and 0.976. Note that the first Fourier mode is absent for S_2. This gap is the mysterious region where no state could be found in the previous study Nagata and Busse (1983).

3.5. Introduction of perturbation $R \neq 0$

In the following, we will show a hidden non-linear branch, both ends of which connect to the non-linear branches emerging from the neutral stability curve $Gr_c(\alpha, 0)$ and the duplications $Gr_c(n\alpha, 0)$ $(n = 2, 3, 4)$. Here, we introduce a perturbation, a small plane Poiseuille flow component, to the system with $R = 0$, by employing a non-zero value of R. As the degenerate spectra are uncovered by the Zeeman effect, it is expected that the introduction of such a perturbation consisting of a net drifting in the streamwise direction will induce a structural instability in the system with $R = 0$, which originally satisfies a relatively higher symmetry. Although the introduced value,

$R = 1$, seems to be subtle, the resulting bifurcation diagram is substantially richer than that obtained by means of the classical step-by-step procedure for the sequential bifurcation. It is of particular interest that the uncovered nonlinear state in the diagram at $R = 1$ survives even when $R = 0$.

3.6. The discovery of the branch T

For example, branch T in Fig.3.3 corresponds to a nonlinear state uncovered in this procedure. The branch T 'fills' the aforementioned gap, which has been previously unexplained properly. This was found systematically by the present procedure utilising the structural instability of the system with $R \neq 0$. We should emphasize that, even at $R = 0$, the branch T possesses a non-zero phase velocity, c, which originates from the system that was perturbed with $R = 1$. Instead if we select the opposite sign of the perturbation, $R = -1$, in the procedure, the same kind of solution drifting in the opposite direction can be obtained. Therefore two drifting solutions have been identified via homotopy followed by its reversal. Extending over the previously unexplained gap, the branch T forms a bridge between the branches, F_+ and S_{3-2}. The contour plot of T is given in Fig.3.4(g) and (h), which are somewhat reminiscent of the vortices in Fig.3.4(c) and (f). This is probably relevant to the existence of the mixed mode suggested by Fujimura and Mizushima Fujimura and Mizushima (1987), even though they obtained evidence of its existence only at a few sets of parameters by weakly nonlinear analysis where the obtained results would be only valid in the vicity of the neutral curves.

3.7. Remainder of nonlinear branches

Our numerical simulations have revealed several more nonlinear branches, which are shown on the left hand side of Fig.3.3. At first, there are additional branches in the region $0.29 \leq \alpha \leq 0.59$, see Fig.3.3. We have only depicted a sample of tertiary states to keep the figure uncluttered. The branch S_n serves as the platform for bifurcation of three higher order distinct branches in the regions, $0.467 \leq \alpha \leq 0.510$, $0.316 \leq \alpha \leq 0.418$, and $0.318 \leq \alpha \leq 0.333$. Moreover, another tertiary state was found in a tiny region $\alpha \approx 0.4712 - 0.4873$. All the branches indicated by thick curve including T possess the phase velocity, which are described in the Fig.3.5.

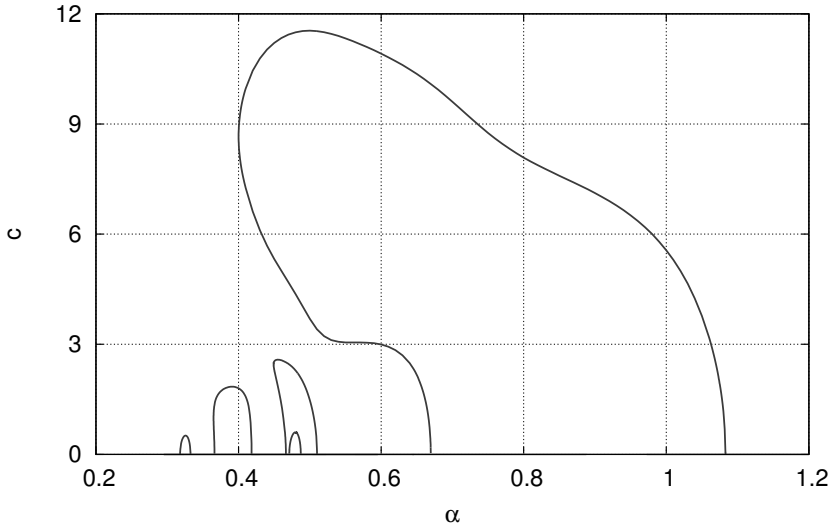

Figure 3.5: Phase velocity for $Gr = 1100$ and $R = 0$.

4. Concluding remarks

4.1. Numerical validation of obtained result

In Table 4.2 we show a comparison between our nonlinear results and those of Mizushima and Saito (1987) for the value of E_1 of (3.12). Despite the different truncation levels employed in the two studies, the results of the corresponding simulations agree to a high degree of accuracy.

4.2. Subcriticality

Additionally, we would like to note a subtle change in bifurcation diagram on $\alpha - Gr$ plane occuring at the wavenumber α_+ between $Gr = 900$ and 1100. The bifurcation of the nonlinear branch, F_+ from the basic state is supercritical at $Gr = 900$. However, beyond a value of Gr between $900 < Gr < 1100$, the bifurcation of nonlinear state F_+ becomes subcritical. This would be better shown in Fig.3.3, where the bifurcation is subcritical, as the existence of region of the nonlinear state moves towards larger wavenumber in the first instance.

Table 4.2: Comparison of nonlinear results with Mizushima and Saito (1987) for the energy E_1 of (3.12) of the pure mode for various (Gr, α) values. In the present work the truncation level $(L, M) = (21, 18)$ has been used for all nonlinear calculations. In Mizushima and Saito (1987) for the nonlinear calculations $L = 40$ was employed with the value of M as indicated.

Gr	α	Mizushima & Saito (M)	Present results ($M = 18$)
500	1.25	2.41706×10^{-4} (4)	2.41746×10^{-4}
500	1.30	2.53302×10^{-3} (4)	2.53306×10^{-3}
600	0.90	9.25916×10^{-4} (6)	9.25916×10^{-4}
600	1.30	6.14480×10^{-2} (6)	6.18481×10^{-2}
2000	2.00	1.88510×10^{-1} (12)	1.88509×10^{-1}
5000	1.30	3.70190×10^{-2} (16)	3.70657×10^{-2}

4.3. Topological change of bifurcation diaggram with increase of Gr

We explain now the topological change of the bifurcation diagram with decreasing of Gr. Although it is not illustrated here, for $Gr = 500$ around the critical Grashof number, the bifurcation of the nonlinear branch is supercritical at $\alpha_\pm$ and has the maximum value in E at $\alpha \approx (\alpha_+ + \alpha_-)/2$, as it is a convex one single curve. The nonlinear branch does not have phase velocity (stationary nonlinear solution).

This is not the case for higher values of Gr. In our study we have found that the single curve of the nonlinear state 'breaks-up' over the bi-critical point, that is, $Gr > Gr_{c,2}$, due to the existence of "resonance". At the bi-critical point where the disconnection occurs, the two split branches are connected with the hidden resonant neutral curve, T. Note that the tertiary branch T exists at smaller Grashof numbers than $Gr_{c,2}$ around S_2.

4.4. Topological change of the bifurcation diagram from $R = 1$ to $R = 0$

Initially the pure mode nonlinear solution, which bifurcates from the neutral curve at $\alpha = 1.9223$ (see Figure 3.3) has a phase velocity ($c = 0.61447$, $\alpha = 1.9223$), (see also Figure 3.3 for comparison), due to the presence of R, follows the path of the pure LHF, but now at $\alpha = 1.06961$ the

pure mode (that bifurcates from the left hand side of the neutral curve) folds and continues within the resonant region, where it connects with the subharmonic $1:2$ resonant mode at $\alpha = 0.8850$. Similarly the solution that bifurcates from the left hand side of the neutral curve at $\alpha = 0.4299$ (with phase velocity ($c = \ 0.48633, \ \ \alpha = 0.42994$), also connects with the $1:2$ resonant mode branch at $\alpha \approx 0.97251$. Therefore the entire branch of the secondary state extends naturally over to the resonant region via two oppositely drifting waves with opposite phase velocities, with both drifting waves connecting with the 1:2 subharmonic (resonant) nonlinear solution. As shown in Figure 3.3, the phase velocities of these two secondary branches (including their loops) are 'bridges' between the disconnected parts of the E_1 curve and the $1:2$ subharmonic (resonant) region for ($Gr = 1100, \ R = 1$) over a range of the wavenumber α.

4.5. Advantage in this procedure : summary

The measure of the influence of the PFC on the bifurcation spectrum of the laterally heated flow without PFC is shown in Fig. 3.3(a), if subsequently we gradually remove the imposed constant pressure gradient. The important aspect here is to note that our calculations have shown that the connecting secondary nonlinear states, extensions of the E_1 curve for the case $R = 1$ and embedded in the resonant region, remain if via homotopy we remove the added value of R and slowly arrive 'back' to the case when there is no PFC, i.e. pure LHF. In other words, while for $R = 1$ there is topologically two $E-$curves, that naturally connect the pure mode (bifurcating from the right and left hand side of the neutral curve) disconnected branches and the resonant bifurcation branches via the introduction of the oppositely moving drifting waves, as shown in Figure 3.3, the topology of the bifurcation tree changes substantially for $R = 0$. The difference (when the constant pressure gradient has been removed, $R = 0$), is that the connecting branches break-up now and the discontinuity points become bifurcation points of higher order, i.e. tertiary, states. The case for $R = 0$, contains a much richer structure than the case $R = 1$, since for the latter the higher order part of the bifurcation is completely absent and only the secondary nonlinear states are present. Without the introduction of the Poiseuille flow perturbation though, we would have not been able to discover the rich structure hidden in the case of $R = 0$.

Acknowledgments. We thank to professors, Kaoru Fujimura (Tottori University, Japan) and Takuji Kawahara (Kansai University, Japan) for discussions and encouragement. TA acknowledges the financial support from Marie Curie Sklodowska Programme of FP7 of the European Union. SG acknowledges financial support from ORDIST of Kansai University, where part of this work was conducted. TI acknowledges a Visiting Scholars fund from Aston University, where this work was completed.

References

Busse, F., Clever, R., 1974. Transition to time dependent convection. J. Fluid Mech. 65, 625–645.

Fujimura, K., Mizushima, J., 1987. Nonlinear interactions of disturbances in free convection between vertical parallel plates. In: Nonlinear wave interactions in fluids. American Society of Mechanical Engineers.

Generalis, S., Fujimura, K., 2009. Range of validity of weakly nonlinear theory in the Rayleigh-Benard problem. J. Phys. Soc. Japan 78 (8), 084401.

Generalis, S., Itano, T., 2010. Characterization of the hairpin vortex solution in plane couette flow. Phys. Rev. E 82 (066308).

Herbert, T., 1980. Nonlinear stability of parallel flows by high order amplitude expansions. AIAA Paper 18 (3), 1125R.

Itano, T., Generalis, S., 2009. Hairpin vortex solution in planar couette flow: Atapestry of knotted vortices. Phys. Rev. Lett. 102 (114501), 4.

Mizushima, J., Fujimura, K., 1992. Higher harminic resonance of two-dimensional disturbances in Rayleigh-Benard convection. J. Fluid Mech. 234 (651-667).

Mizushima, J., Saito, Y., 1987. Equilibrium characteristics of the secondary convection in a vertical fluid layer between two flat plates. Fl.Dyn.Res. 2, 183–191.

Nagata, M., Busse, F., 1983. Three-dimensional tertiary motions in a plane shear layer. J. Fluid Mech. 135, 1–26.

Squire, H., 1933. On the stability of three-dimensional disturbances of viscous flow between parallel walls. Proc. Roy. Soc. A142, 129–155.